Nanoscale

PAPER

View Article Online
View Journal

Cite this: DOI: 10.1039/c7nr07300c

Low-force spectroscopy on graphene membranes by scanning tunneling microscopy†

Bernd Uder, *[a] Haibin Gao,[a] Peter Kunnas,[b] Niels de Jonge[b] and Uwe Hartmann[a]

Received 30th September 2017,
Accepted 1st January 2018

DOI: 10.1039/c7nr07300c

rsc.li/nanoscale

Two-dimensional atomically flat sheets with a high mechanical flexibility are very attractive as ultrathin membranes but are also inherently challenging for microscopic investigations. We report on a method using Scanning Tunneling Microscopy (STM) under ultra-high vacuum conditions for non-indenting low-force spectroscopy on micrometer-sized freestanding graphene membranes. The method is based on applying quasi-static voltage ramps with active feedback at low tunneling currents and ultimately relies on the attractive electrostatic force between the tip and the membrane. As a result a bulge-test scenario can be established. The convenience and simplicity of the method relies on the fact that the loading force and the membrane deflection detection are both provided simultaneously by the STM. This permits the continuous measurement of the stress–strain relation. Electrostatic forces applied are typically below 1 nN and the membrane deflection is detected at sub-nanometer resolution. Experiments on single-layer graphene membranes with a strain of 0.1% reveal a two-dimensional elastic modulus E_{2D} = 220 N m^{-1}.

1 Introduction

The experiments on graphene in 2004 boosted research on two-dimensional (2D) materials.[1,2] Among the many extraordinary properties of graphene, its high mechanical strength makes it a possible candidate for nanomechanical applications. Nanoelectromechanical systems (NEMS) in terms of resonators using graphene sheets have been realized,[3,4] but the quality factors are still much lower than for SiC oscillators.[5] Graphene's chemical stability combined with its mechanical flexibility renders it also interesting as a separation membrane. Experiments have shown that nanoporous graphene is suitable for desalination processes.[6] Indentation experiments by Atomic Force Microscopy (AFM) revealed a two-dimensional Young's modulus of E_{2D} = 340 N m^{-1} in agreement with theory.[7–9] Counterintuitive are findings of higher values (550 N m^{-1}) for graphene with a relatively low defect density.[10] Graphene always shows deviations from the ideal 2D structure.[11] Static ripples were measured by Transmission Electron Microscopy (TEM) and by STM.[12,13] Bulge tests with electrostatically pressured graphene and a deflection detection by interferometric profilometry revealed a softening of crumpled graphene with a reduced Young's modulus of E_{2D} = (20–100) N m^{-1}.[14] Furthermore a strain dependence of E_{2D} was found on pressurized graphene membranes.[15] This somehow agrees with atomistic calculations, but a difference of a factor of two between measured and calculated values remained.[16] Dual-probe STM revealed the capability of a tip in tunneling contact to modify the graphene landscape[17] and it was found that STM is able to control the curvature of freestanding graphene.[18–20] In the following we report a technique which utilizes a tip in tunneling contact at low currents and with tip–sample forces below 1 nN to realize a bulge-test scenario, to control the strain and to measure simultaneously the membrane deflection at sub-nanometer resolution.

2 Experimental

STM experiments were realized with a modified commercial ultra-high vacuum (UHV) STM operating at room temperature.[21,22] Samples consist of CVD-on-Cu-grown single layer graphene transferred to a perforated Formvar®/carbon support with circular holes covering a TEM gold grid (mesh 300).[23,24] The quality of a production batch of the CVD-grown graphene was checked on a Si/SiO_2 substrate by Raman spectroscopy and optical inspection.[25] Samples were mounted *ex situ* and subsequently introduced into the UHV system. Imaging was performed without further sample treatment in UHV. It was found that samples imaged hours (typically >24 h) after introduction into the UHV system at pressures of $p < 10^{-8}$ mbar without baking do not reveal changes over time. Normal water-degassing rates in the UHV chamber are sufficient to remove moisture from samples which were previously exposed to

[a]Institute of Experimental Physics, Saarland University, Saarbruecken, D-66041, Germany. E-mail: bernd.uder@uni-saarland.de
[b]INM - Leibniz Institute for New Materials, Saarbruecken, D-66123, Germany

†Electronic supplementary information (ESI) available: Additional information to SEM & AFM imaging and force calibration. See DOI: 10.1039/C7NR07300C

ambient conditions. Experiments of heat-treated samples showed that such a treatment can affect the membrane quality. Scanning Electron Microscopy (SEM) was used to inspect the STM tips prior to the introduction into the UHV chamber. The tip radius (r) was typically 50 nm. Tips were tested on highly oriented pyrolytic graphite (HOPG) for atomic resolution imaging and they were routinely conditioned using standard voltage pulsing techniques. Force spectroscopy was realized by recording the vertical tip position (z) in tunneling contact as a function of the applied sample bias (V) with active feedback. The tunneling current (I) was typically set to 10 pA. This corresponds to a tunneling distance of z_0 = 1.2 nm at V = 0.1 V as obtained by $z(I)$ experiments on HOPG.† A quasi-static $z(V)$ spectroscopy was realized by using low slew rates at typically 22 mV s^{-1}. I was always recorded in parallel to z and additionally monitored by an oscilloscope during the entire experiment. Samples have been complimentarily characterized by high-resolution SEM (ThermoFischer, Quanta 250 ESEM) using a Everhart–Thornley Detector and by ambient-air AFM (DI Multimode).

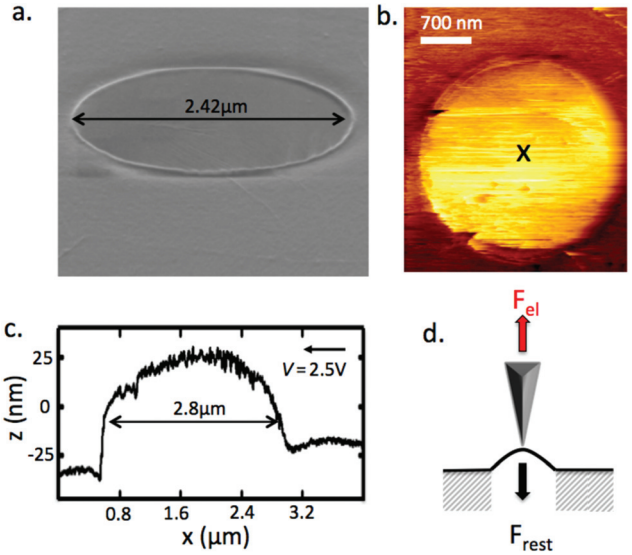

Fig. 1 (a) SEM image of a graphene-covered hole. The magnification was 120 000×, the electron beam energy was 5 keV, and the specimen was tilted by an angle of 75° (b) STM image of a graphene membrane: V = 1.1 V, I = 40 pA, line-scan frequency 3 Hz, tip-scan speed 8.4 μm s^{-1}, loop gain 26%, image recorded in 6 min. (c) Typical STM profile scan across a membrane: V = 2.5 V, I = 100 pA, loop gain 2%, line recorded in 40 s. The arrow indicates the scan direction. The membrane diameter seen in STM is increased with respect to the SEM result due to a combination of scanner calibration and the convolution of tip and hole shape. (d) Sketch of the bulge-test scenario with the electrostatic force F_{el} and the restoring force F_{rest} of the deformed membrane.

3. Results and disussion

3.1 Spectroscopy with active feedback

Graphene membranes for spectroscopy were imaged and selected by high-speed STM mapping at high loop gain.[22] Fig. 1 shows a typical SEM image and the STM map of a graphene-covered hole.

High-resolution SEM reveals a hole diameter of 2.42 μm and a sharp edge at the rim.† STM line-profile scans at a high V (Fig. 1(c)) show a steep rise of approximately 25 nm followed by a smoothly curved shape towards the membrane center. AFM images with the tip and the sample at ground potential reveal a similar behavior at the membrane edge, but a flat profile across the membrane.† This is a clear proof showing that a tip electrostatically pulling at the center is able to lift the whole membrane. Profile scans at different V always yield identical values for the membrane diameter and confirm that the graphene film is not being detached at the rim during STM experiments.

A bulge-test scenario was realized by pulling at the membrane center utilizing $z(V)$ spectroscopy. The electrostatic force F_{el} is proportional to V^2 and is always attractive. In the following we refer to the absolute value of V. With increasing V the membrane is pulled towards the tip until a balance of F_{el} and a restoring force F_{rest} is reached (Fig. 1(d)). Changes of the vertical tip position z at constant I with active feedback can reach several tens of nanometers and are by far too large to be explained solely by changes of the local density of states.[18,19] The tip at constant I must follow the vertical membrane position and $z(V)$ data are thus suited to detect the deflection of the membrane. Ten successively at the membrane center recorded $z(V)$ curves are shown in Fig. 2. Each cycle starts with a ramp from −1.2 V to −0.1 V (release direction) immediately followed by a ramp back to −1.2 V (pull direction). A characteristic and reproducible shape is seen in all curves. The curves are reversible but they show a hysteresis between pull and release directions for voltages between −0.5 V and −0.75 V. Remarkable are large changes of z with amplitudes of approximately 30 nm. A similar behavior was found in previous STM investigations and it was explained by ripple flipping with transitions between a rippled and a flat graphene configuration.[19,26] STM experiments at 4 K on graphene drumheads permit the conclusion that van der Waals forces between tip and membrane are the dominant pull-up forces causing substantial deformations. However, tunneling current settings were not specified leaving the question of the distance between the tip and the membrane open.[27] The series of measurements presented in Fig. 2 at a tunneling distance† of 1.2 nm clearly proofs that the electrostatic force is the dominant pulling force.

A representative curve is shown in Fig. 3 in more detail together with the simultaneously recorded I. Correlating z and I verifies that the large changes of z are not due to artifacts of the distance regulation. I is stable at 10 pA and small fluctuations with amplitudes below 120 pA are only seen at low V. Changes of z appear differently for the pull and the release directions. An abrupt change (*flip down*) is seen for the release direction with a transition time of approximately 0.6 s. The correlation of z and I data (see inset of Fig. 3) implies a loss of the tunneling contact just before the *flip down* occurs. This is followed by a tip approach until tunneling is established

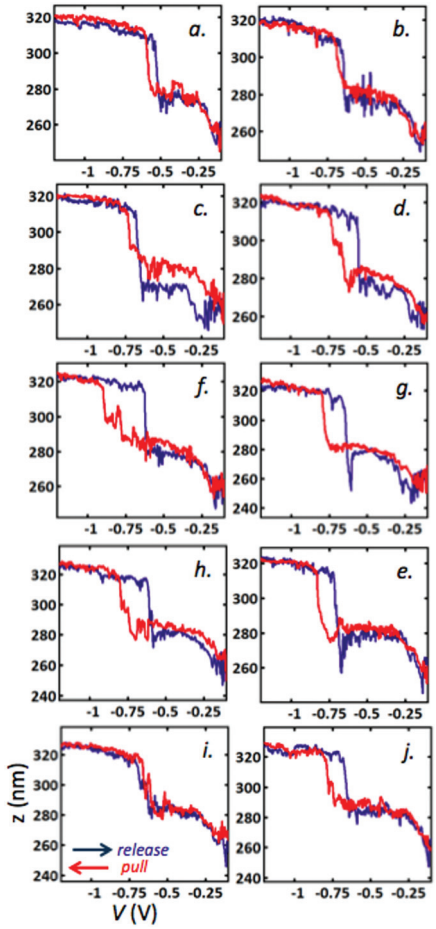

Fig. 2 Series of ten successive $z(V)$ experiments with active feedback at the membrane center. V starts at −1.2 V, is incremented in 500 steps (slew rate = 22 mV s^{-1}) to −0.1 V (release direction) and then ramped back from −0.1 V to −1.2 V (pull direction). Each ramping direction involves 500 data points with 100 ms per data point at a sampling rate of 440 kHz. The arrows in (i) indicate the ramp directions. Tunneling parameter: I = 10 pA, loop-gain 2%. The total measurement time (a–j) is 17 min.

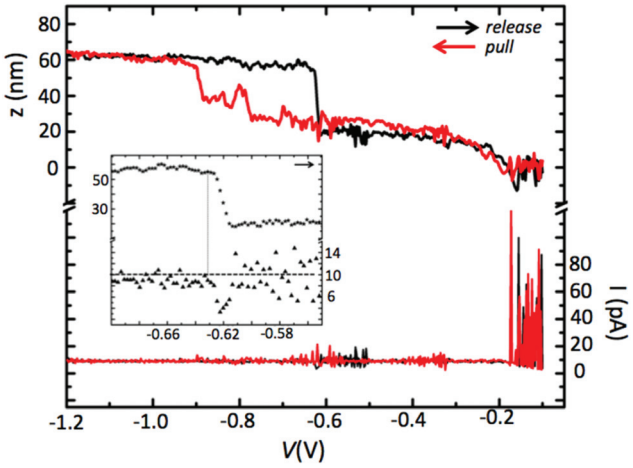

Fig. 3 Details from a typical curve of Fig. 2. The arrows indicate the ramp directions: I = 10 pA, loop-gain 2%. Slew rate 22 mV s^{-1}. Inset: Zoom of the flip down with z and I data. The time per pixel is 100 ms.

again. Pulling exhibits a cascade-like transition (*flip ups*). Correlating z and I data reveals an interplay between I and the integral distance controller[22] with iterative tip-retract and approach cycles until a stable position is reached. The total height change between −1.2 V and −0.1 V of approximately 60 nm corresponds to the maximum deflection seen in the line profile measured at high V (Fig. 1(c)). *Flip-down* and *flip-up* positions can vary and sometimes no hysteresis is seen [Fig. 2 (b and i)]. Local time-dependent experiments recording z over time† show aperiodic membrane fluctuations with amplitudes of 1–2 nm at low voltages that are highly likely to trigger the loss of the tunneling contact. These fluctuations cause a random error of the flip position.

3.2 Force calibration

Approximating the geometry of the STM tip by a sphere of radius r at a close distance z_0 above a plane surface yields a relation between the applied voltage V_0 and the electrostatic force[28]

$$F_{\mathrm{el}} = -\frac{\pi\varepsilon_0 {V_0}^2 r}{z_0}. \quad (1)$$

The vacuum permittivity is $\varepsilon_0 = 8.85 \times 10^{-12}$ A^2 s^4 kg^{-1} m^{-3}. A correction of the tunneling distance z_0 is necessary due to an increasing tunneling-current contribution with rising V. For low voltages Ohm's law is applicable to the tunnel junction.[29,30] Including this in the exponential distance dependence of the tunneling current, the electrostatic force F_{el} between the STM tip and the graphene membrane is given by

$$F_{\mathrm{el}} = -\frac{\pi\varepsilon_0 V^2 r}{z_0(1+\ln(V/V_0))}. \quad (2)$$

The tip radius is r = (50 ± 10) nm and the tunneling distance at a sample bias of V_0 = −0.1 V is z_0 = (1.2 ± 0.1) nm. The membrane deflection is defined by $h = z(V) - z_0(1 + \ln(V/V_0))$. The force calibration (eqn (2)) is applied to the $z(V)$ data of the pull direction of curve (*j*) of Fig. 2.† Force-*versus*-deflection data are shown in Fig. 4.

Four different regions are distinguishable in the relation between the electrostatic force F_{el} and the membrane deflection h. Region I exhibits a deflection of approximately 15 nm for fairly low forces. Further force increase (region II) deflects the membrane only by a few nanometers before a force above a threshold of −0.15 nN is causing large and cascade-like changes of h with a total amplitude of approximately 30 nm. The slope changes again at the beginning of region IV. The region III corresponds to the *flip up*- and *flip down* processes with a hysteresis as seen in the measurement series of Fig. 2.

3.3 Bulge-test scenario

While the experimental set-up of a bulge test is simple, the interpretation is often complicated.[31] One challenge is to

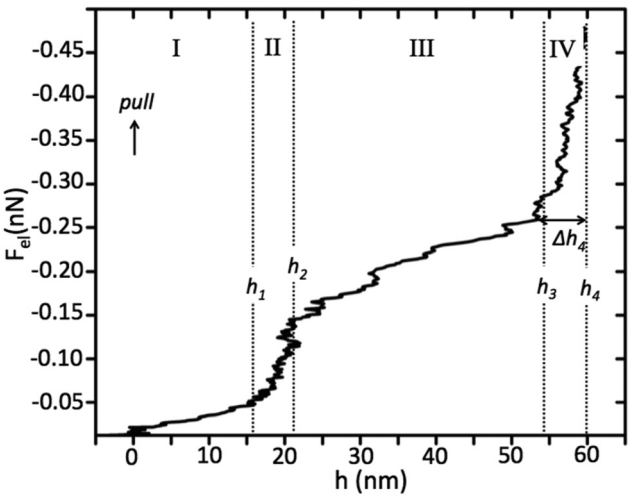

Fig. 4 Relation between electrostatic force F_{el} and membrane deflection h from the $z(V)$ curve of Fig. 2(j).

identify the experimental boundary conditions. In particular if the membrane is slack prior to curving, interpretation of the obtained data is difficult.

In the present spectroscopy experiments a characteristic relation between the applied electrostatic force F_{el} and the membrane deflection h is seen in the experimental data (Fig. 2 and 4). This permits a better knowledge of the membrane shape when applying the bulge test.

In the following a model (Fig. 5(a–d)) is presented to explain different membrane conditions and to relate them to the experimental data of Fig. 4. The circular holes in the substrate have a characteristic sharp edge with a height of approximately 25 nm as seen in high-resolution SEM images and they

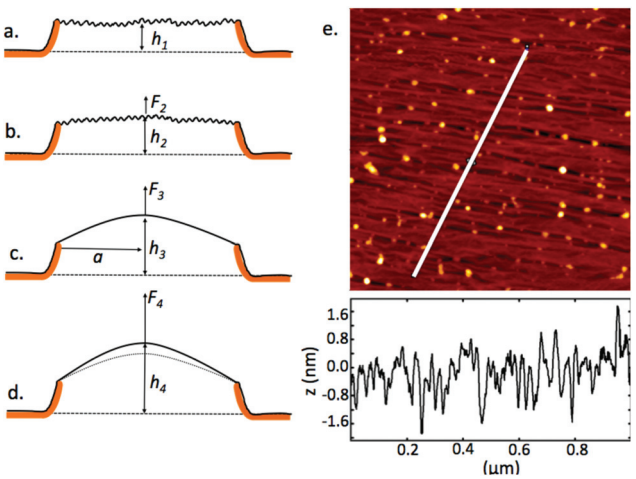

Fig. 5 (a–d) Schematic representation of a membrane with radius a and a sharp edge of the substrate hole: (a) a slack rippled membrane. (b) A rippled membrane without slackness. (c) A ripple-free and curved membrane. (d) The deflection of a ripple-free and curved membrane. (e) AFM image of a graphene-membrane with static ripples. The profile is along the white line.

are covered by the graphene layer (Fig. 1(a)). The shape of the hole covered by the membrane is confirmed by AFM, Laser-Scanning Microscopy and White-Light Interferometry experiments. AFM images show static ripples (Fig. 5(e)) on the freestanding membrane but not on membranes on top of the substrate. The bright dots seen in the AFM image are most likely due to chemical residuals from the sample preparation and are seen on the freestanding membrane and the graphene layer on top of the substrate.

Without a pulling force the rippled membrane is slack above the hole with an average height h_1 above the substrate level (Fig. 5(a)). A force F_2 eliminates the slackness and lifts the membrane to a height h_2 (Fig. 5(b)). Static ripples still exist, but the rippled membrane is now taut. Increasing the force removes the ripples and the membrane reaches a height h_3 at a force F_3 (Fig. 5(c)). Further pulling by a force F_4 deflects the membrane (Fig. 5(d)) and bulge-test equations should be applicable. If a pressure of $P = F_{el}/\pi a^2$ is applied to a circular membrane, the in-plane stress σ_r and the radial strain ε_r are given by[14,31]

$$\sigma_r = \frac{Pa^2}{4\Delta h} \quad (3)$$

$$\varepsilon_r = \frac{2\Delta h^2}{3a^2} \quad (4)$$

with the membrane radius a and the bulge height Δh. When Hooke's law is applicable the in-plane Young's modulus is given by $E_{2D} = (1 - \nu)\sigma_r/\varepsilon_r$. This results in a cubic relation between F_{el} and the bulge height Δh.

$$F_{el} = \frac{8}{3\pi}\frac{E_{2D}}{(1-\nu)a^2}\Delta h^3 \quad (5)$$

A Poisson ratio of $\nu = 0.275$ is used for the micrometer-sized membrane.[16] Eqn (5) is applied to the experimental data of region IV in Fig. 4. This corresponds to the membrane condition of Fig. 5(d). The bulge height is defined as $\Delta h = h - h_3$. The strain of the membrane at position h_3 is obtained from $\varepsilon_r = 2(h_3 - h)^2/(3a^2)$. The force calibration (eqn (2)) was applied to all curves shown in Fig. 2. The resulting force-*versus*-deflection data are shown in Fig. 6 separately for the release and the pull directions.

In contrast to Fig. 4 vertical and horizontal axes are exchanged in Fig. 6 for a better comparison of the individual curves. Clearly visible is a good agreement of the release and pull directions in region IV. The data analysis yields $\Delta h_4 = (6.5 \pm 0.5)$ nm for a maximum pulling force of $F_{el} = 0.48$ nN. At the lift height h_3 the membrane is strained with a deflection of $h_3 - h_1 = (48 \pm 5)$ nm. The membrane radius obtained from high-resolution SEM is $a = (1210 \pm 20)$ nm. Applying eqn (4) and (5) yields $E_{2D} = (220 \pm 120)$ N m^{-1} and $\varepsilon_r = (0.10 \pm 0.02)\%$.

3.4 Accuracy of the method

The accuracy of the force calibration in the experiments is approximately 30% and is strongly influenced by uncertainties of the tip radius. With a better control over the tip shape a pre-

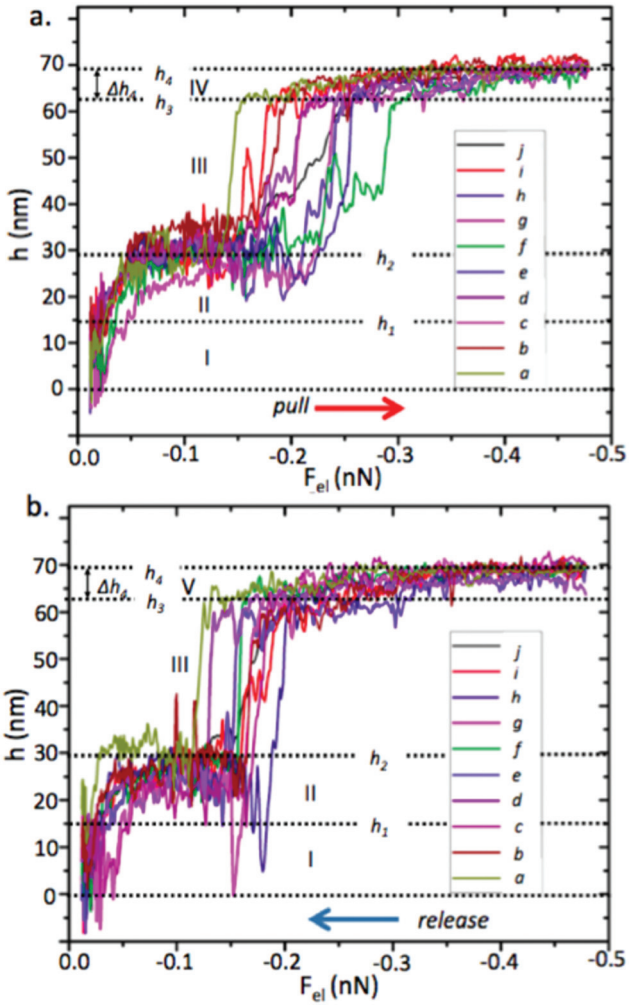

Fig. 6 Force–deflection data of the experimental series shown in Fig. 2. The data have been corrected to remove a constant vertical drift. (a) Release data (V from −1.2 V to −0.1 V) (blue curves in Fig. 2). (b) Pull data (V from −0.1 V to −1.2 V) (red curves in Fig. 2). The maximum applied force is 0.48 nN at V = −1.2 V.

cision of F_{el} below 15% is realistic coming close to the precision of spring calibration methods for AFM cantilevers.[32] Apart from the precision of the force calibration, the accuracy to determine E_{2D} depends on the detection of the strained membrane state (position h_3 in Fig. 6) which can be improved by increasing the number of pull and release cycles.

4 Conclusions

We have shown that the subtle interaction between a tip and an atomically thin graphene membrane in tunneling contact can be used for nonindenting force spectroscopy. Quasi-static force spectroscopy is achieved by applying a slow sample bias ramp at a low tunneling current to deflect the membrane and to simultaneously monitor the deflection by STM. The capability to apply forces below 1 nN in a nonindenting set-up is well-suited to control the membrane deflection. Thus a bulge-test scenario on atomically thin membranes can be realized in a straightforward way. The method was applied to a strained freestanding single-layer of graphene and permitted the detection of Young's modulus. The value obtained agrees with atomistic calculations.[16] Theoretical and experimental investigations yield divergent values of the Young's modulus of an atomically thin graphene membrane.[33–36] This clearly indicates the principle challenge to determine a macroscopic property of a monolayer system. Experimental techniques, as for example indentation with high forces, are prone to tamper results by the risk to modify the system or by nonlinear effects. The presented technique at low forces reduces these risks and therefore offers an alternative route to investigate monolayer systems in a smooth and reversible manner.

Conflicts of interest

There are no conflicts to declare.

Acknowledgements

We thank E. Arzt for his support through INM.

References

1 K. S. Novoselov, A. K. Geim, S. V. Morozov, D. Jiang, Y. Zhang, S. V. Dubonos, I. V. Grigorieva and A. A. Firsov, *Science*, 2004, **306**, 666–669.
2 Q. Tang and Z. Zhou, *Prog. Mater. Sci.*, 2013, **58**, 1244–1315.
3 J. S. Bunch, A. M. van der Zande, S. S. Verbridge, I. W. Frank, D. M. Tanenbaum, J. M. Parpia, H. G. Craighead and P. L. McEuen, *Science*, 2007, **315**, 490–493.
4 C. Chen, Ph.D. Thesis, Columbia University, 2013.
5 X. L. Feng, C. J. White, A. Hajimiri and M. L. Roukes, *Nat. Nanotechnol.*, 2008, **3**, 342–346.
6 S. P. Surwade, S. N. Smirnov, I. V. Vlassiouk, R. R. Unocic, G. M. Veith, S. Dai and S. M. Mahurin, *Nat. Nanotechnol.*, 2015, **10**, 459–464.
7 C. Lee, X. Wei, J. W. Kysar and J. Hone, *Science*, 2008, **321**, 385–388.
8 R. Al-Jishi and G. Dresselhaus, *Phys. Rev. B: Condens. Matter Mater. Phys.*, 1982, **26**, 4514–4522.
9 K. N. Kudin, G. E. Scuseria and B. I. Yakobson, *Phys. Rev. B: Condens. Matter Mater. Phys.*, 2001, **64**, 235406.
10 G. Lopez-Polin, C. Gomez-Navarro, V. Parente, F. Guinea, M. I. Katsnelson, F. Perez-Murano and J. Gomez-Herrero, *Nat. Phys.*, 2015, **11**, 26–31.
11 A. Fasolino, J. H. Los and M. I. Katsnelson, *Nat. Mater.*, 2007, **6**, 858–861.
12 J. C. Meyer, A. K. Geim, M. I. Katsnelson, K. S. Novoselov, T. J. Booth and S. Roth, *Nature*, 2007, **446**, 60–63.

13 R. Zan, C. Muryn, U. Bangert, P. Mattocks, P. Wincott, D. Vaughan, X. Li, L. Colombo, R. S. Ruoff, B. Hamilton and K. S. Novoselov, *Nanoscale*, 2012, **4**, 3065–3068.
14 R. J. Nicholl, H. J. Conley, N. V. Lavrik, I. Vlassiouk, Y. S. Puzyrev, V. P. Sreenivas, S. T. Pantelides and K. I. Bolotin, *Nat. Commun.*, 2015, **6**, 8789.
15 G. Lopez-Polin, M. Jaafar, F. Guinea, R. Roldan, C. Gomez-Navarro and J. Gomez-Herrero, 2015, arXiv:1504.05521v1 [cond-mat.mtrl-sci].
16 J. H. Los, A. Fasolino and M. I. Katsnelson, *Phys. Rev. Lett.*, 2016, **116**, 015901.
17 F. R. Eder, J. Kotakoski, K. Holzweber, C. Mangler, V. Skakalova and J. C. Meyer, *Nano Lett.*, 2013, **13**, 1934–1940.
18 P. Xu, Y. Yang, S. D. Barber, M. L. Ackerman, J. K. Schoelz, D. Qi, I. A. Kornev, L. Dong, L. Bellaiche, S. Barraza-Lopez and P. M. Thibado, *Phys. Rev. B: Condens. Matter Mater. Phys.*, 2012, **85**, 121406.
19 R. Breitwieser, Y.-C. Hu, Y. C. Chao, R.-J. Li, Y. R. Tzeng, L.-J. Li, S.-C. Liou, K. C. Lin, C. W. Chen and W. W. Pai, *Carbon*, 2014, **77**, 236–243.
20 R. Breitwieser, Y.-C. Hu, Y. C. Chao, Y. R. Tzeng, S.-C. Liou, K. C. Lin, C. W. Chen and W. W. Pai, *Phys. Rev. B: Condens. Matter Mater. Phys.*, 2017, **96**, 085433.
21 *Omicron VT STM and Matrix control system*, http://www.scientaomicron.com/en/home.
22 B. Uder and U. Hartmann, *Rev. Sci. Instrum.*, 2017, **88**, 063702.
23 Graphenea, San Sebastian, Spain, http://www.graphenea.com.
24 Quantifoil, Jena, Germany, http://www.quantifoil.com.
25 A. Zurutuza, Graphenea, San Sebastian, Spain, private communications, 2016.
26 M. Neek-Amal, P. Xu, J. K. Schoelz, M. L. Ackerman, S. D. Barber, P. M. Thibado, A. Sadeghi and F. M. Peeters, *Nat. Commun.*, 2014, **5**, 4962.
27 N. N. Klimov, S. Jung, S. Zhu, T. Li, C. A. Wright, S. D. Solares, D. B. Newell, N. B. Zhitenev and J. A. Stroscio, *Science*, 2012, **336**, 1557–1561.
28 F. J. Giessibl, *Rev. Mod. Phys.*, 2003, **75**, 949–983.
29 J. G. Simmons, *J. Appl. Phys.*, 1963, **34**, 1793–1803.
30 U. Hartmann, *Nanostrukturforschung und Nanotechnologie: Band 1 Grundlagen*, Gruyter Studium, 2012.
31 M. K. Small and W. Nix, *J. Mater. Res.*, 1992, **7**, 1553–1563.
32 N. A. Burnham, X. Chen, C. S. Hodges, G. A. Matei, E. J. Thoreson, C. J. Roberts, M. C. Davies and S. J. B. Tendler, *Nanotechnology*, 2003, **14**, 1.
33 F. Memarian, A. Fereidoon and M. D. Ganji, *Superlattices Microstruct.*, 2015, **85**, 348–356.
34 D. G. Papageorgiou, I. A. Kinloch and R. J. Young, *Prog. Mater. Sci.*, 2017, **90**, 75–127.
35 J.-U. Lee, D. Yoon and H. Cheong, *Nano Lett.*, 2012, **12**, 4444–4448.
36 S. Deng and V. Berry, *Mater. Today*, 2016, **19**, 197–212.

